Year: 2020

Enhanced prognostic stratification of neoadjuvant treated lung squamous cell carcinoma by computationally-guided tumor regression scoring

Casanova, Ruben ; Leblond, Anne-Laure ; Wu, Chengguang ; Haberecker, Martina ; Burger, Irene A ; Soltermann, Alex

Abstract: INTRODUCTION The amount of residual tumor burden after neoadjuvant chemotherapy is an important prognosticator, but for non-small cell lung carcinoma (NSCLC), no official regression scoring system is yet established. Computationally derived histological regression scores could provide unbiased and quantitative readouts to complement the clinical assessment of treatment response. METHODS Histopathologic tumor regression was microscopically assessed on whole cases in a neoadjuvant chemotherapy-treated cohort (NAC, n = 55 patients) of lung squamous cell carcinomas (LSCC). For each patient, the slide showing the least pathologic regression was selected for subsequent computational analysis and histological features were quantified: percentage of vital tumor cells (cTu.Percentage), total surface covered by vital tumor cells (cTu.Area), area of the largest vital tumor fragment (cTu.Size.max), and total number of vital tumor fragments (cTu.Fragments). A chemo-naïve LSCC cohort (CN, n = 104) was used for reference. For 23 of the 55 patients [^{18}F]-Fluorodeoxyglucose (FDG) PET/CT measurements of maximum standard uptake value (SUV_{max}), background subtracted lesion activity (BSL) and background subtracted volume (BSV) were correlated with pathologic regression. Survival analysis was carried out using Cox regression and receiver operating characteristic (ROC) curve analysis using a 3-years cutoff. RESULTS All computational regression parameters significantly correlated with relative changes of BSV FDG PET/CT values after neoadjuvant chemotherapy. ROC curve analysis of histological parameters of NAC patients showed that cTu.Percentage was the most accurate prognosticator of overall survival (ROC curve AUC = 0.77, p-value = 0.001, Cox regression HR = 3.6, p = 0.001, variable cutoff $<= 30$ %). CONCLUSIONS This study demonstrates the prognostic relevance of computer-derived histopathologic scores. Additionally, the analysis carried out on slides displaying the least pathologic regression correlated with overall pathologic response and PET/CT values. This might improve the objective histopathologic assessment of tumor response in neoadjuvant setting.

DOI: https://doi.org/10.1016/j.lungcan.2020.07.003

Originally published at:
Casanova, Ruben; Leblond, Anne-Laure; Wu, Chengguang; Haberecker, Martina; Burger, Irene A; Soltermann, Alex (2020). Enhanced prognostic stratification of neoadjuvant treated lung squamous cell carcinoma by computationally-guided tumor regression scoring. Lung Cancer, 147:49-55.
DOI: https://doi.org/10.1016/j.lungcan.2020.07.003

Lung Cancer 147 (2020) 49–55

Contents lists available at ScienceDirect

Lung Cancer

journal homepage: www.elsevier.com/locate/lungcan

Enhanced prognostic stratification of neoadjuvant treated lung squamous cell carcinoma by computationally-guided tumor regression scoring

Ruben Casanova[a,*], Anne-Laure Leblond[a], Chengguang Wu[a], Martina Haberecker[a], Irene A. Burger[b], Alex Soltermann[c]

[a] Institute of Pathology and Molecular Pathology, University Hospital Zurich, Switzerland
[b] Department of Nuclear Medicine, University Hospital Zurich, Switzerland
[c] ADMED Pathology, Neuchâtel, Switzerland

ARTICLE INFO

Keywords:
Lung
Squamous cell carcinoma
Neoadjuvant chemotherapy
Computational pathology
Prognosis

ABSTRACT

Introduction: The amount of residual tumor burden after neoadjuvant chemotherapy is an important prognosticator, but for non-small cell lung carcinoma (NSCLC), no official regression scoring system is yet established. Computationally derived histological regression scores could provide unbiased and quantitative readouts to complement the clinical assessment of treatment response.

Methods: Histopathologic tumor regression was microscopically assessed on whole cases in a neoadjuvant chemotherapy-treated cohort (NAC, n = 55 patients) of lung squamous cell carcinomas (LSCC). For each patient, the slide showing the least pathologic regression was selected for subsequent computational analysis and histological features were quantified: percentage of vital tumor cells (cTu.Percentage), total surface covered by vital tumor cells (cTu.Area), area of the largest vital tumor fragment (cTu.Size.max), and total number of vital tumor fragments (cTu.Fragments). A chemo-naïve LSCC cohort (CN, n = 104) was used for reference. For 23 of the 55 patients [^{18}F]-Fluorodeoxyglucose (FDG) PET/CT measurements of maximum standard uptake value (SUV_{max}), background subtracted lesion activity (BSL) and background subtracted volume (BSV) were correlated with pathologic regression. Survival analysis was carried out using Cox regression and receiver operating characteristic (ROC) curve analysis using a 3-years cutoff.

Results: All computational regression parameters significantly correlated with relative changes of BSV FDG PET/CT values after neoadjuvant chemotherapy. ROC curve analysis of histological parameters of NAC patients showed that cTu.Percentage was the most accurate prognosticator of overall survival (ROC curve AUC = 0.77, p-value = 0.001, Cox regression HR = 3.6, p = 0.001, variable cutoff < = 30 %).

Conclusions: This study demonstrates the prognostic relevance of computer-derived histopathologic scores. Additionally, the analysis carried out on slides displaying the least pathologic regression correlated with overall pathologic response and PET/CT values. This might improve the objective histopathologic assessment of tumor response in neoadjuvant setting.

1. Introduction

In a neoadjuvant setting, the administration of chemotherapy before surgery may result in significant reduction of the tumor burden, thus enabling radical resection in otherwise not operable patients. This treatment strategy has been shown to improve both overall (OS) [1] and recurrence-free survival (RFS) in resectable non-small cell lung carcinoma (NSCLC) [2]. Neoadjuvant chemotherapy induces distinctive morphological changes of both tumor and stromal compartments of solid carcinomas. This often results in significant reduction of tumor burden, which is accompanied by an increase of fibrotic stroma and necrosis as well as an increased infiltration by foamy cell macrophages [3].

Although there is no WHO-accepted consensus for regression scoring of NSCLC [4], the extent of residual vital tumor epithelia together with the amount of fibrosis are important prognostic parameters [5]. Several regression scoring systems have been proposed for this tumor based on the percentage of remaining tumor cells [6–8] or the residual tumor area [9]. However, most scoring methods rely on a semi-quantitative and visual pathologic evaluation of the residual tumor burden on H&E stained whole sections. Therefore, accurate quantification of morphologic parameters including amount and size of residual

* Corresponding author at: Ruben Casanova, Department of Quantitative Biomedicine, University of Zurich, Winterthurerstrasse 190, 8057 Zurich, Switzerland.
E-mail address: ruben.casanova@uzh.ch (R. Casanova).

https://doi.org/10.1016/j.lungcan.2020.07.003
Received 15 April 2020; Received in revised form 19 June 2020; Accepted 2 July 2020
Available online 03 July 2020

tumor tissue could be useful for improving and standardizing current NSCLC regression schemes [10]. Junker et al. proposed a regression scheme in 3 grades starting from a grade 1 defined as no or only spontaneous regression, a grade 2 as incomplete regression (2a with > 10 %, 2b with ≤10 % vital tumor cells) and grade 3 as complete regression without any detectable vital tumor cells [6,7]. Following these results, it has been shown that NSCLC with less than 10 % of residual vital tumor cells [8,11], a histopathological complete remission (CR) [12,13] or a total area of residual tumor (ART) ≤400 mm^2 [9] were favorable prognostic parameters. Thus, the automatic quantification of morphologic parameters could be a good indicator of the effectiveness of therapy in NSCLC [10].

The field of tissue diagnostics is witnessing substantial changes with the recent approval of Whole Slide Imaging (WSI) for primary diagnosis [14] and the rapid development of not only information management systems but also digital image analysis tools encompassing immunohistochemical staining scoring, detection of regions of interest displaying abnormalities and other prognostic algorithms. Hence, computational pathology has the potential to integrate routine pathology workflow and reduce pathologist's workload by performing time-consuming tasks [15,16].

We have previously developed an image analysis approach to quantify tumor fragmentation [17] in lung squamous cell carcinoma (LSCC), the second most common histological subtype of NSCLC [18]. This structural feature was associated with increased tumor invasion and poor prognosis. Herein, we have extended our approach to evaluate the potential clinical relevance of four computerized morphologic parameters related to the residual tumor burden in a cohort of 55 neoadjuvant treated (NAC) LSCC. We investigated the prognostic value of computational tumor regression scoring in comparison to conventional histopathologic regression scoring and further evaluated their correlation with [^{18}F]- Fluorodeoxyglucose (FDG)PET/CT-based tumor metabolic activity parameters.

2. Materials and methods

2.1. Patient cohorts

In this retrospective study, patients with diagnosed primary LSCC at the University Hospital Zurich were selected. Patients with synchronic or metachronic second primary tumor, with overall survival (OS) < 1 month post-surgery and/or with incomplete clinical data were excluded. Squamous cell differentiation according to WHO criteria was assessed on hematoxylin-eosin (H&E) stains and verified by alcian blue-periodic acid schiff (AB-PAS) histochemistry as well as TTF1, p40, CK7 and synaptophysin immunohistochemistry (IHC) for poorly differentiated LSCC. The neoadjuvant chemotherapy group (NAC cohort) consisted of 55 patients diagnosed with LSCC with a median follow-up time of 51 months (range: 2–141). In total 19 patients received gemcitabine-platinum chemotherapy, 26 taxane-platinum and 10 other combinations. Chemotherapy cycles ranged from two to five (2 cycles: n = 3, 3 cycles n = 43, 4 cycles: n = 7, 5 cycles: n = 2. Histopathological regression after neoadjuvant chemotherapy was evaluated by microscopy by two observers simultaneously on H&E tissue sections. The tumor regression grade (TRG) was evaluated on all available tissue blocks and referred to the amount of non-vital tumor tissue induced by the chemotherapy - characterized by the presence of extensive necrosis and fibrosis, foamy cells reactions and cholesterol crystals - in relation to the remaining vital tumor cells. TRG was evaluated as follows : complete pathologic response (CPR, 0% of remaining tumor cells), major pathologic response (MPR, < 10 % remaining tumor cells) and minor pathologic response (IPR > 10 % remaining tumor cells) similar to [5]. The chemo-naïve cohort (CN) consisted of 104 patients with a median follow-up time of 52 months (range: 2–137). The ethical commission of the Canton of Zurich approved the study under reference number KEK ZH-Nr. 29-2009/14.

2.2. Histopathological samples preparation

For each neoadjuvant treated case, one tissue block with the highest amount of residual tumor tissue (i.e. the least pathologic regression) was selected for pan-cytokeratin IHC. For the chemo-naïve cases, two representative tumor blocks were selected to perform a comparative analysis. Tissue sections of 2 µm thickness were prepared for the selected tumor blocks and IHC was performed using mouse monoclonal anti-human cytokeratin AE1/AE3 (M3515, DAKO, dilution 1:50) on an automated platform (Ventana Medical Systems, Tucson, AZ, USA). The following detection was finalized with a secondary antibody and the OptiView DAB kit (Ventana Medical Systems). IHC stained sections were scanned using a high-resolution whole slide scanner (Nanozoomer Digital Pathology, Hamamatsu, Japan) using a 40x objective and downscaled to a spatial resolution of 0.23 µm/pixel. Tumor tissue was manually annotated by a surgical pathologist (A.S.) in order to exclude surrounding non-tumor lung tissue from the analysis.

2.3. Image processing and regression scoring

For the CN cohort, a color threshold was used to segment malignant tumor tissue (brown positive signal) from its surrounding desmoplastic stroma (blue-grey counterstain) using Fiji [19], as described [17]. Morphologic parameters of the segmented tumor tissue were retrieved for each tumor specimen and computed as following: 1. percentage of vital tumor cells (cTu.Percentage = tumor cells area/[tumor cells area + stroma area]*100), 2. total surface covered by vital tumor cells (cTu.Area), 3. size of the largest vital tumor fragment (cTu.Size.max), 4. total number of vital tumor fragments (cTu.Fragments), defined as disconnected carcinoma fragment larger than 800 μm^2, separated by stroma. As chemo-treated cases often show extensive necrosis or unspecific staining, tissue segmentation of vital tumor epithelia versus necrosis and/or unspecific stromal staining was performed by a trainable algorithm using the software inForm Tissue Finder™ (PerkinElmer, Waltham, MA, USA).

2.4. FDG PET/CT acquisition and analysis

Patients from the NAC cohort with available FDG PET/CT before and after neoadjuvant treatment (before tumor resection) were analyzed. FDG PET/CT selection criteria were: fasting for at least 4 h, no elevated blood glucose, adequate FDG injection (difference < 100 MBq between both FDG injections), FDG uptake time within 45 − 60 min and acceptable image quality. For a total of 23 patients, pre and post-neoadjuvant chemotherapy images were available. The detailed protocol is explained in our previous study [20]. Metabolic tumor activity was measured following the instructions as described [21] and was performed without knowledge of regression scores. The maximum Standard Uptake Value (SUV_{max}), background subtracted lesion activity (BSL) and background subtracted volume (BSV) were considered in this analysis. In brief, a volume of interest was placed around the primary tumor, including the entire tumor activity without regions of physiologically increased activity (e.g. FDG-uptake of the heart). Within the selected VOI SUV_{max}, BSL and BSVusing a background adapted threshold for each lesion were measured [22]. The relative change in FDG-PET metrics between post- and pre-neoadjuvant chemotherapy was calculated ($dSUV_{max,}$ dBSL and dBSV).

2.5. Data interpretation and statistical analysis

All statistical analyses were performed on SPSS version 25 software (SPSS Inc., Chicago, USA), R version 3.5.0 and R-studio version 1.1.383. Overall survival (OS) and relapse-free survival (RFS) were evaluated from the date of surgery to the date of death or documented relapse, as described [23]. Only patients with no evidence of remaining tumor after surgical resection of the primary tumor (R0) were included in RFS

calculations. Quantitative morphologic differences between neoadjuvant chemo-treated (NAC) and chemo-naïve (CN) groups were addressed using the Wilcoxon signed-rank test. Correlations between the FDG PET/CT metrics (SUV_{max}, BSL and BSV) and the morphologic parameters (cTu.Percentage, cTu.Area, cTu.Size.max, cTu.Fragments) were calculated using the non-parametric Spearman's rank correlation test. A receiver operator characteristic (ROC) curve was generated for each morphologic parameter using a cutoff of 3-year OS and RFS to separate short and long-term survivors. The area under the ROC curve (AUROC) was computed for each parameter. Patients with clinical follow-up shorter than 3 years were omitted in the ROC analysis. The optimal cutoff point was determined for each parameter with the point that minimizes the distance to the top-left corner in the ROC plane as described [24]. Kaplan-Meier curve p-values were calculated using the log-rank test. Hazard ratios were retrieved by univariate Cox regression. Ordinal categorical variables were coded using Reverse Helmert coding (each level of categorical variable is compared to the mean of the previous level). P-values < 0.05 were considered significant.

3. Results

3.1. Neoadjuvant treatment induces significant morphologic changes in LSCC tissue

Morphologic changes after neoadjuvant treatment were addressed by comparing the NAC cohort with the untreated CN group. In total four computerized morphologic parameters representing the percentage of tumor cells within the tumor area (cTu.Percentage), the total tumor cells surface (cTu.Area), the largest fragment (cTu.Size.max) and the total number of tumor fragments (cTu.Fragments) were quantified by image-based morphometric analysis for all LSCC cases (Fig. 1A–C). The distribution of these morphometric parameters was significantly different between the two cohorts and all four parameters were considerably reduced in the NAC compared to CN group (all p-values < 0.001) (Fig. S1, A–H). Histological examples of NAC LSCCs showing different regression patterns are shown in Fig. 1(D–F).

Within the NAC group, morphologic alterations were compared between gemcitabine-platinum ($n = 19$) and taxane-platinum ($n = 26$) regimens excluding other treatment combinations. Results showed that cTu.Area and cTu.Size.max values were lower for the taxane-platinum treated group, using the non-parametric Mann-Whitney *U* test ($p = 0.040$ and $p = 0.009$, respectively) (Figure S2).

3.2. Computerized histological regression scoring improves LSCC prognostic stratification

The distribution of clinic-pathologic parameters for the NAC and CN cohorts is summarized in Table 1. The CN cohort showed similar clinical parameters distributions. In the NAC cohort particularly, age, ypN, ypM and stage were prognostic parameters whereas no survival difference was observed between different chemotherapy regimens ($p = 0.239$).

To better compare the prognostic relevance of clinical and computational parameters, ROC analysis was performed with patients stratified into short-term and long-term survival, using a threshold of 3-year OS. In the NAC cohort, 22 and 33 patients were respectively grouped like this. In the CN cohort, 37 and 67 patients were split into short and long-term OS. The results for the NAC cohort showed that the parameters cTu.Percentage, cTu.Area, and cTu.Size.max were able to significantly stratify patients in two risk groups, using a 3-year OS cutoff, whereas cTu.Fragments was not prognostic (Fig. 2, A). The parameters cTu.Area and cTu.Size.max were consistently prognostic using a 3-year RFS cutoff point (Figure S3). In contrast, for CN patients, cTu.Percentage, cTu.Area, and cTu.Size.max were not significant parameters whereas cTu.Fragments was the best discriminative morphologic parameter using 3-year OS and RFS cutoffs (Figure S4).

Following these results, further clinical analysis was conducted on the NAC cohort focusing on clinic-pathologic parameters. ROC analysis showed that stage, ypN and TRG were able to stratify patients in two risk groups, whereas ypT was not significant (Figure S5). Stage and ypN showed the highest area under the ROC (AUROC) and were comparable with the computational parameter cTu.Percentage. Similar results were found using a 3-year RFS cutoff (Figure S3, B). Additionally, univariate cox regression was performed for all computational parameters as well as most relevant clinico-pathologic parameters, dichotomized at their optimal cutoff point (Table 2). High cTu.Percentage and cTu.Size.max values were significantly associated with decreased OS, whereas cTu.Area, cTu.Fragments and TRG scores were not significantly prognostic ($p > 0.05$). Kaplan Meier survival curves are shown in Fig. 2(B–G).

3.3. Computational histological regression correlates with relative FDG PET/CT metabolic changes before and after neoadjuvant chemotherapy

The correlation of histopathological regression with tumor metabolic activity was addressed using pre- and post-NAC FDG PET/CT scans. Relative changes between pre- and post-chemo were also considered in the analysis (delta values). Histopathological regression was evaluated using all four computational parameters (cTu.Percentage, cTu.Area, cTu.Size.max, and cTu.Fragments) in addition to the conventional TRG scores.

The comparison of pre-NAC, post-NAC and the corresponding relative changes (delta-NAC) FDG PET/CT parameters showed, that post-NAC FDG PET/CT volumetric values (BSL and BSV) positively correlated with all computational parameters whereas pre-NAC FDG PET/CT values did not show any significant correlation with any tumor regression parameter (Fig. 3). Among all FDG PET/CT values, the volume-based metric dBSV correlated best with all regression parameters on both post-NAC and delta-NAC settings. Both post-NAC and delta-NAC SUV_{max} significantly correlated with c.Tu.Percentage and TRG only. Among the computed regression parameters, cTu.Percentage was the only one consistently correlating with all FDG PET/CT parameters post NAC.

4. Discussion

In this study we proposed an approach to quantify tumor regression in lung squamous cell carcinoma after neoadjuvant chemotherapy by computational pathology. Four computational histo-morphologic parameters related to the residual tumor burden were quantified using pan-cytokeratin immunohistochemistry and compared to the pathologic response using a three-tiered tumor regression scoring system assessed by the pathologist on H&E stained whole section microscopy. Correlations with FDG PET/CT values and clinical outcome were assessed in order to address the potential clinical relevance of quantitative tumor regression readouts for routine response assessment after neoadjuvant therapy.

We focused our study on the morphologic changes induced by NAC in a cohort of lung squamous cell carcinoma (LSCC). Unlike adenocarcinoma which grows in five distinct morphologic patterns [25], LSCC is histologically characterized by the presence of solid tumor epithelia sheets of varying size and cohesiveness displaying various degrees of keratinization [26]. Our morphometric analysis showed that cTu.Percentage, cTu.Area, cTu.Size.max and cTu.Fragments were all significantly decreased in neoadjuvant chemotherapy treated patients when compared to a chemo-naïve cohort. Moreover, survival analysis showed that high residual cTu.Percentage, cTu.Area and cTu.Size.max values after neoadjuvant chemotherapy were markers of poor prognosis. In contrast, these parameters were not prognostic in the chemo-naïve setting, whereas cTu.Fragments, a parameter reflecting tumor invasiveness, was prognostic only in this group of patients. This also suggests that computational histo-morphologic parameters may allow

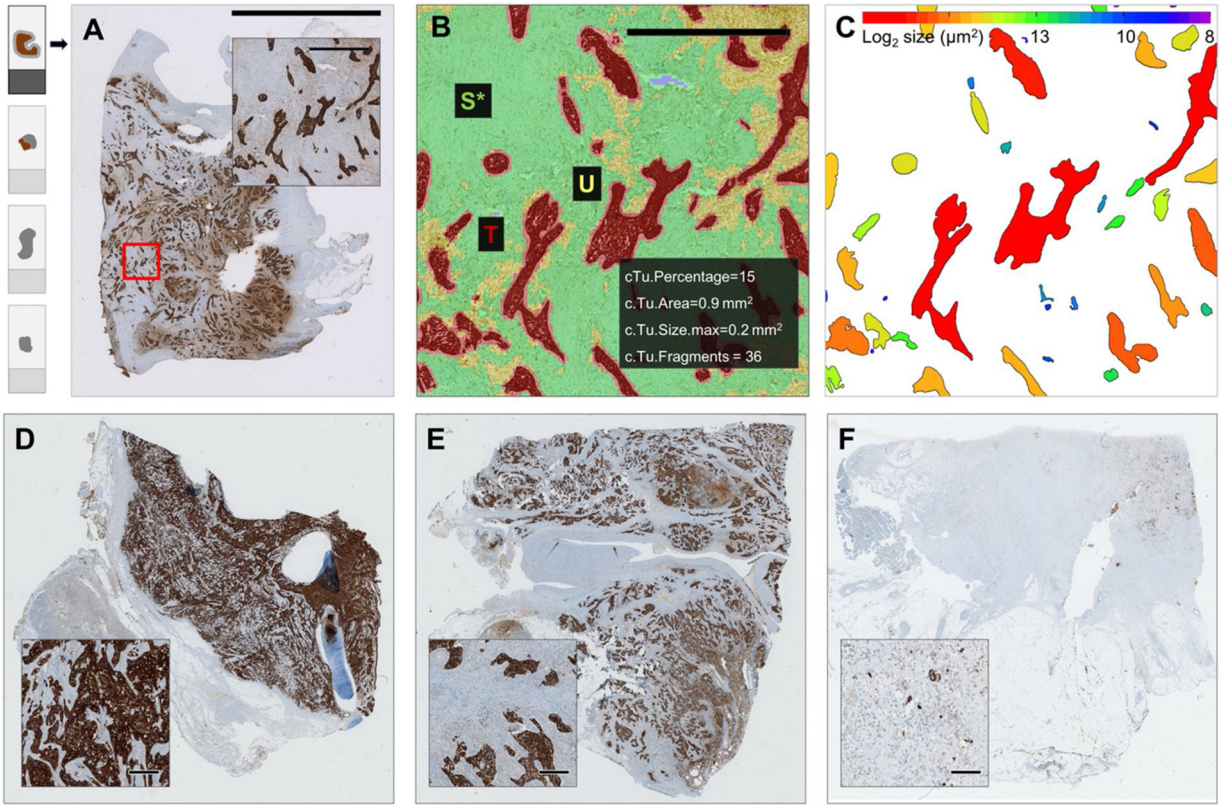

Fig. 1. Computerized morphometric analysis. A) Overview of a lung squamous cell carcinoma stained by pan-cytokeratin IHC. Scale bar: 10 mm. Left: Corresponding schematic of the sampling strategy. The top section represents the slide with the least regression (i.e. highest amount of residual tumor tissue) selected for morphometric analysis. (Legend: brown = vital tumor content, grey = regressed tumor area without vital tumor cells. Top-right: magnified area of interest, scale bar: 1 mm. B) Corresponding tissue detection (overlay) after trainable tissue region segmentation. Legend: T = tumor tissue (red); S = stroma (green); U = unspecific staining (yellow), accounting for stroma. C) Analysis of tumor fragments i.e. connected tumor regions and corresponding masks colored by size in µm^2. D-F) Histological example of NAC treated LSCCs showing different degrees of tumor regression (D) IPR with no signs of regression, (E) IPR with minor signs of regression, (F) MPR with < 10 % vital tumor cells. Scale bar = 200 µm.

Table 1
Univariate Cox regression analysis and summary of clinico-pathologic parameters.

Clinicopathologic parameters		Neoadjuvant chemo-treated (NAC) n = 55						Chemo-naïve (CN) n = 104				
		N	%	HR	CI (95 %)	p		N	%	HR	CI (95 %)	p
Age	range: 40 – 76 years					**0.049**	**Age**	range: 40 – 87 years				0.207
	≤median (61)	28	(51 %)	1.0	–	–		≤median (65)	55	(53 %)	1.0	–	–
	> median	27	(49 %)	1.4	(1.0 – 2.0)	0.049		> 65	49	(47 %)	1.3	(0.8 – 2.2)	0.207
Sex						0.897	**Sex**						0.190
	female	12	(22 %)	1.0	–	–		female	21	(20 %)	1.0	–	–
	male	43	(78 %)	1.1	(0.45 – 2.47)	0.897		male	83	(80 %)	0.7	(0.4 – 1.2)	0.190
ypT						0.658	**pT**						**< 0.001**
	0	5	(9%)	1.0	–	–							
	1	19	(34 %)	3.4	(0.4 – 26.7)	0.241		1	24	(23 %)	1.0	–	–
	2	13	(24 %)	1.5	(0.4 – 5.3)	0.498		2	34	(33 %)	1.203	(0.6 – 2.4)	0.604
	3	7	(13 %)	1.8	(0.5 – 6.9)	0.412		3	34	(33 %)	1.827	(1.1 – 3.1)	0.027
	4	11	(20 %)	1.9	(0.7 – 5.0)	0.199		4	12	(12 %)	3.787	(2.0 – 7.3)	< 0.001
ypN						**0.010**	**pN**						0.075
	0	26	(47 %)	1.0	–			0	49	(47 %)	1.0	–	–
	1	20	(37 %)	0.9	(0.4 – 2.1)	0.795		1	34	(33 %)	1.808	(1.1 – 3.1)	0.032
	2 – 3	9	(16 %)	3.7	(1.6 – 8.7)	0.002		2 – 3	21	(20 %)	1.24	(0.7 – 2.2)	0.462
ypM						**0.014**	**pM**						**< 0.001**
	0	54	(98 %)	1.0	–	–		0	100	(96 %)	1.0	–	–
	1a-c	1	(2%)	17.3	(1.8 – 166.55)	0.014		1a-c	4	(4%)	27.0	(7.6 – 95-7)	< 0.001
Stage						**0.005**	**Stage**						**< 0.001**
	0	5	(9 %)	1.0	–	–							
	I	13	(23 %)	**2.3**	(0.3 – 18.6)	0.450		I	26	(25 %)	1.0	–	–
	II	14	(26 %)	**1.4**	(0.4 – 5.0)	0.629		II	38	(37 %)	1.4	(0.7 – 2.8)	0.326
	III	22	(40 %)	**4.1**	(1.6 – 10.6)	0.004		III	36	(35 %)	2.2	(1.3 – 3.7)	0.002
	IV	1	(2%)	**27.5**	(2.7 – 280.3)	0.005		IV	4	(4%)	30.1	(8.4 – 107.4)	< 0.001

Legend: NAC = neoadjuvant chemotherapy; CN = chemo-naive; HR = hazard ratio; CI = 95 % confidence interval; p(T/N/M) = pathologic evaluation (y) after neoadjuvant chemotherapy.

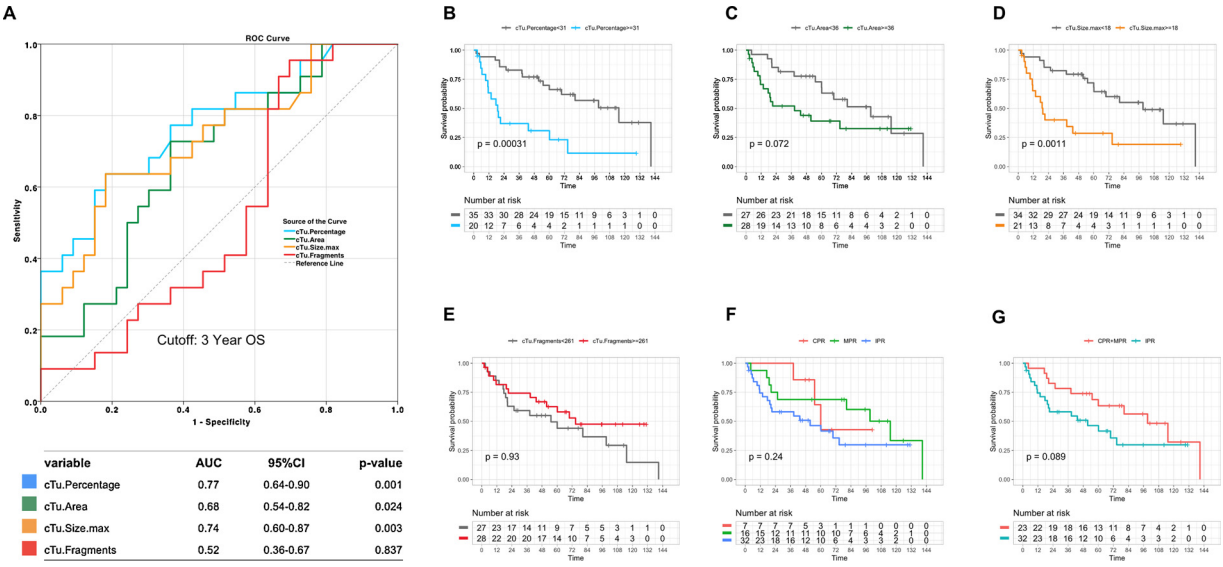

Fig. 2. ROC curves and survival analysis of morphologic parameters for neoadjuvant-treated patients. A) Receiver operator characteristic (ROC) curves for the status 3-year overall survival using computational morphologic parameters (C-Parameters) for all NAC patients. B-G) Kaplan Meier survival curves for all C-Parameters as well as histopathological TRG scores (CPR = complete pathologic response, MPR = major pathologic response, IPR = minor pathologic response). AUC = area under the curve; CI = confidence interval; cTu.Percentage = percentage of tumor cells within the whole tumor tissue; cTu.Area = vital tumor cells area [mm]; cTu.Size.max = area of the largest fragment [mm]; cTu.Fragments = number of tumor fragments separated by stroma; time = months.

Table 2
Cox regression analysis of morphologic parameters.

Variables	Univariate		
	HR	CI (95 %)	p-value
cTu.Percentage $_{<\ 31}$	**3.6**	(1.7–7.5)	**0.001**
cTu.Area $_{<\ 36}$	**1.9**	(0.9–3.9)	0.077
cTu.Size.max $_{<\ 18}$	**3.0**	(1.5–6.4)	**0.003**
cTu.Fragments $_{<\ 261}$	**0.6**	(0.3–1.3)	0.230
TRG (CPR + MPR vs IPR)	**1.9**	(0.9–4.0)	0.094
	multivariate		
	HR	CI (95 %)	p-value
Stage $_{0\text{-II vs III-IV}}$	**2.6**	(1.1–6.1)	**0.028**
cTu.Percentage $_{<\ 31}$	**2.6**	(1.2–5.8)	**0.016**

Top: cox univariate analysis using the computational morphologic parameters cTu.Percentage, cTu.Area, cTu.Size.max, cTu.Fragments dichotomized at the best cutoff point. TRG = pathological tumor regression grade, dichotomized. Bottom: multivariate cox regression using the dichotomized Stage (0, I, II vs III-IV) and cTu.Percentage (cutoff = 31). Legend: HR = hazard ratio; CI = 95 % confidence interval, CPR = complete pathologic response, MPR = major pathologic response, IPR = minor pathologic response.

for differential tumor grading for patients having received chemotherapy prior to surgical resection. In this study, although computational morphologic parameters were highly correlated with each other, ROC analysis showed that cTu.Percentage was the most relevant qualifier for the stratification of patients into high and low risks categories, using a 3-year OS cutoff. When compared to clinical parameters, cTu.Percentage showed similar performances than tumor stage and lymph node involvement as well as better performances than TRG scores described in [6,7].

FDG PET/CT is a valuable imaging modality to predict histological response after neoadjuvant therapy [27]. In our study, PET/CT-morphometry correlation analysis was performed using the SUV_{max} in addition to two volume-based PET values accounting for the lesion activity (BSL) and the metabolic tumor volume (BSV) as metrics of tumor metabolic activity. Our analysis showed that computed regression parameters correlated best with BSV for both post-NAC and delta-NAC FDG PET/CT, whereas SUV_{max} was only associated with the percentage of residual tumor cells and TRG scores. This could be potentially relevant when reporting PET/CT values, since the metabolically active tumor volume could better reflect histological features compared to SUV_{max}. Not surprisingly, our analysis showed that, overall, pre-NAC FDG PET/CT values did not correlate with the measured histological parameters. This is in line with previous studies, showing that the change of standardized uptake values correlate with histopathologic responses in NSCLC [28–33] whereas pre-chemo PET/CT is likely to be insufficient to predict pathologic response in LSCC [30].

Our study has nonetheless limitations. The morphometric analysis was performed using the tissue block showing the least pathologic regression and pan-cytokeratin IHC, whereas following the most recent recommendations, pathologic response to therapy should include all H &E slides of tumor [5]. For this reason, our cTu.Percentage scores are virtually higher and cannot be directly compared with previously published pathologic scores. However, our survival analysis showed that regression scores done on the histological cut section displaying the least regression pattern, was significantly prognostic and showed better prediction performances than TRG scores. Follow-up studies could assess whether the least histological regression would be a better prognosticator than evaluating tumor regression over the whole tumor area for LSCC. Additionally, our study focused solely on squamous cell carcinoma of the lung, which is a subtype of NSCLC. Adenocarcinomas are grouped into five morphologic subtypes: lepidic, acinar, papillary, micropapillary and solid [25]. These morphologic patterns significantly affect FDG uptake [34] and it has been shown that squamous cell carcinomas have higher SUV uptake than adenocarcinomas [35–39]. Therefore, in order to study a homogeneous population by morphometrics and PET analyses, only LSCC were selected in our study. Finally, we presented here a retrospectively study. To determine whether computerized regression scoring could serve as surrogate histopathological response assessment with clinical benefit, larger validation studies would be required.

5. Conclusions

The field of pathology is witnessing substantial transformations, with the growing acceptance of whole slide imaging for full sign-out of

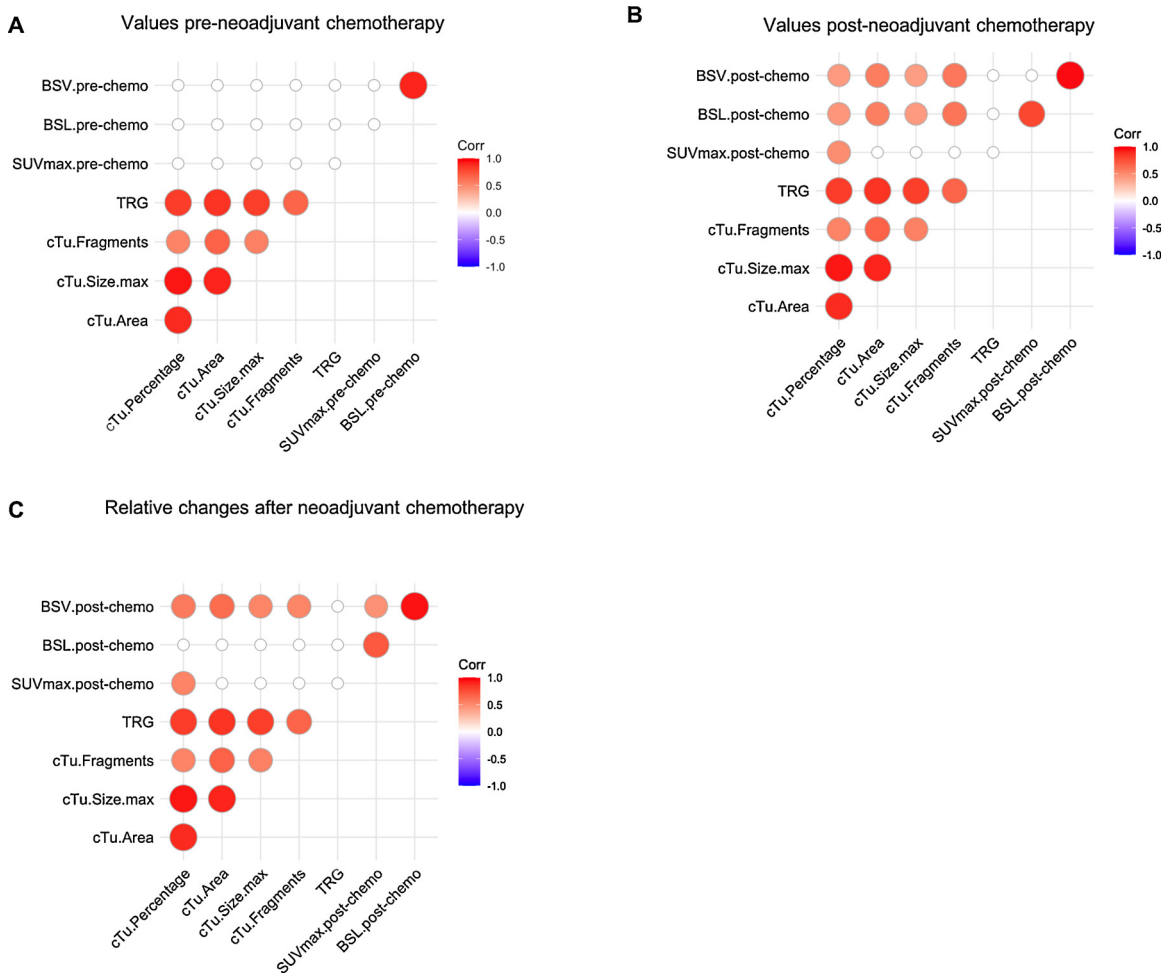

Fig. 3. Correlation matrix of ^{18}F-FDG PET/CT with morphologic C-parameters. Computational morphologic scores as well as histopathological regression scoring TRG were correlated with PET values before and after NAC treatment (n = 23 patients). Correlations of histological parameters include the whole NAC cohort (n = 55). Correlation coefficients (Corr) are indicated with the corresponding color-scale: blue = negative, red = positive. Delta = relative changes between post-chemo and pre-chemo values; SUV_{max} = maximum standard uptake value; BSV = metabolic tumor volume; BSL = total lesion glycolysis; TRG = tumor regression score (CPR, MPR, IPR); cTu.Percentage = percentage of tumor cells within the whole tumor tissue; cTu.Area = vital tumor cells area [mm^2]; cTu.Size.max = area of the largest fragment [mm^2]; cTu.Fragments = number of tumor fragments separated by stroma; white circles = p-values > 0.05.

diagnostic surgical pathology [40] and the accelerated development of computational pathology applications. Artificial intelligence algorithms capable of detecting lymph node metastases on histological images from breast cancer patients [41,42], or able to predict histopathological parameters as well as patient outcome using histological sections [43–48] are few examples of prospective opportunities of computational pathology to assist pathologists in their daily routine. Reproducibility studies are currently needed to better assess pathologic response in the neoadjuvant setting and computational approaches could play major role in harmonizing pathologic response readouts [5]. In our study, we have proposed a digital pathology approach for accurate histopathologic assessment of tumor regression after neoadjuvant chemotherapy and curative surgery. This approach is not restricted to LSCC nor to a specific type of treatment. It has the potential to be applied to larger clinical studies who would benefit from reproducible and quantitative histological readouts of treatment response. The histopathologist would thereby obtain an additional independent computerized regression score.

Funding

Swiss Cancer League (reference number F-87701-31-01), Swiss Commission of Technology and Innovation CTI (reference number 25736-1 PFLS-LS).

CRediT authorship contribution statement

Ruben Casanova: Conceptualization, Methodology, Investigation, Formal analysis, Writing - original draft, Writing - review & editing. **Anne-Laure Leblond:** Data curation, Investigation, Writing - review & editing. **Chengguang Wu:** Formal analysis. **Martina Haberecker:** Data curation, Validation. **Irene A. Burger:** Resources, Supervision, Writing - review & editing. **Alex Soltermann:** Resources, Supervision, Conceptualization, Funding acquisition, Writing - review & editing.

Declaration of Competing Interest

The authors declare to have no competing financial interest.

Acknowledgements

We would like to acknowledge Dr. Karina Silina (Institute of Experimental Immunology, University of Zurich) and Dr. Dimitri Korol (Cancer Registry, University Hospital Zurich) for their support. This study was funded by Swiss Cancer League (reference number F-87701-31-01) and Swiss Commission of Technology and Innovation CTI

(reference number 25736-1 PFLS-LS).

Appendix A. Supplementary data

Supplementary material related to this article can be found, in the online version, at doi:https://doi.org/10.1016/j.lungcan.2020.07.003.

References

[1] W.A. Song, N.K. Zhou, W. Wang, X.Y. Chu, C.Y. Liang, X.D. Tian, et al., Survival benefit of neoadjuvant chemotherapy in non-small cell lung cancer: an updated meta-analysis of 13 randomized control trials, J. Thorac. Oncol. 5 (4) (2010) 510–516.

[2] Group NM-aC, Preoperative chemotherapy for non-small-cell lung cancer: a systematic review and meta-analysis of individual participant data, Lancet 383 (9928) (2014) 1561–1571.

[3] X. Liu-Jarin, M.B. Stoopler, H. Raftopoulos, M. Ginsburg, L. Gorenstein, A.C. Borczuk, Histologic assessment of non-small cell lung carcinoma after neoadjuvant therapy, Mod. Pathol. 16 (11) (2003) 1102–1108.

[4] M.D. Hellmann, J.E. Chaft, W.N. William Jr., V. Rusch, K.M. Pisters, N. Kalhor, et al., Pathological response after neoadjuvant chemotherapy in resectable non-small-cell lung cancers: proposal for the use of major pathological response as a surrogate endpoint, Lancet Oncol. 15 (1) (2014) e42–50.

[5] W.D. Travis, S. Dacic, I. Wistuba, L. Sholl, P. Adusumilli, L. Bubendorf, et al., IASLC multidisciplinary recommendations for pathologic assessment of lung cancer resection specimens after neoadjuvant therapy, J. Thorac. Oncol. 15 (5) (2020) 709–740.

[6] K. Junker, M. Thomas, K. Schulmann, F. Klinke, U. Bosse, K.M. Muller, Tumour regression in non-small-cell lung cancer following neoadjuvant therapy. Histological assessment, J. Cancer Res. Clin. Oncol. 123 (9) (1997) 469–477.

[7] K. Junker, K. Langner, F. Klinke, U. Bosse, M. Thomas, Grading of tumor regression in non-small cell lung cancer : morphology and prognosis, Chest 120 (5) (2001) 1584–1591.

[8] A. Pataer, N. Kalhor, A.M. Correa, M.G. Raso, J.J. Erasmus, E.S. Kim, et al., Histopathologic response criteria predict survival of patients with resected lung cancer after neoadjuvant chemotherapy, J. Thorac. Oncol. 7 (5) (2012) 825–832.

[9] Y. Yamane, G. Ishii, K. Goto, M. Kojima, M. Nakao, Y. Shimada, et al., A novel histopathological evaluation method predicting the outcome of non-small cell lung cancer treated by neoadjuvant therapy: the prognostic importance of the area of residual tumor, J. Thorac. Oncol. 5 (1) (2010) 49–55.

[10] M. Goto, M. Naito, K. Saruwatari, K. Hisakane, M. Kojima, S. Fujii, et al., The ratio of cancer cells to stroma after induction therapy in the treatment of non-small cell lung cancer, J. Cancer Res. Clin. Oncol. 143 (2) (2017) 215–223.

[11] C.C. Vu, R. Matthews, B. Kim, D. Franceschi, T.V. Bilfinger, W.H. Moore, Prognostic value of metabolic tumor volume and total lesion glycolysis from (1)(8)F-FDG PET/CT in patients undergoing stereotactic body radiation therapy for stage I non-small-cell lung cancer, Nucl. Med. Commun. 34 (10) (2013) 959–963.

[12] C. Pottgen, M. Stuschke, B. Graupner, D. Theegarten, T. Gauler, V. Jendrossek, et al., Prognostic model for long-term survival of locally advanced non-small-cell lung cancer patients after neoadjuvant radiochemotherapy and resection integrating clinical and histopathologic factors, BMC Cancer 15 (2015) 363.

[13] B. Milleron, V. Westeel, V. Gounant, M. Wislez, E. Quoix, Pathological complete response: a predictive survival factor after neoadjuvant chemotherapy in lung cancer, Bull. Cancer 103 (1) (2016) 66–72.

[14] Food and Drug Administration, FDA Allows Marketing of First Whole Slide Imaging System for Digital Pathology, (2018) (page last updated: 28/03/2018), https://www.fda.gov/newsevents/newsroom/pressannouncements/ucm552742.htm.

[15] B.J. Williams, D. Bottoms, D. Treanor, Future-proofing pathology: the case for clinical adoption of digital pathology, J. Clin. Pathol. 70 (12) (2017) 1010–1018.

[16] J. Griffin, D. Treanor, Digital pathology in clinical use: where are we now and what is holding us back? Histopathology 70 (1) (2017) 134–145.

[17] R. Casanova, D. Xia, U. Rulle, P. Nanni, J. Grossmann, B. Vrugt, et al., Morphoproteomic characterization of lung squamous cell carcinoma fragmentation, a histological marker of increased tumor invasiveness, Cancer Res. 77 (10) (2017) 2585–2593.

[18] S. Francisci, P. Minicozzi, D. Pierannunzio, E. Ardanaz, A. Eberle, T.K. Grimsrud, et al., Survival patterns in lung and pleural cancer in Europe 1999-2007: results from the EUROCARE-5 study, Eur. J. Cancer (2015).

[19] J. Schindelin, I. Arganda-Carreras, E. Frise, V. Kaynig, M. Longair, T. Pietzsch, et al., Fiji: an open-source platform for biological-image analysis, Nat. Methods 9 (7) (2012) 676–682.

[20] I.A. Burger, R. Casanova, S. Steiger, L. Husmann, P. Stolzmann, M.W. Huellner, et al., 18F-FDG PET/CT of non-small cell lung carcinoma under neoadjuvant chemotherapy: background-based adaptive-volume metrics outperform TLG and MTV in predicting histopathologic response, J. Nucl. Med. 57 (6) (2016) 849–854.

[21] I.A. Burger, H.A. Vargas, A. Apte, B.J. Beattie, J.L. Humm, M. Gonen, et al., PET quantification with a histogram derived total activity metric: superior quantitative consistency compared to total lesion glycolysis with absolute or relative SUV thresholds in phantoms and lung cancer patients, Nucl. Med. Biol. 41 (5) (2014) 410–418.

[22] I.A. Burger, H.A. Vargas, B.J. Beattie, D.A. Goldman, J. Zheng, S.M. Larson, et al., How to assess background activity: introducing a histogram-based analysis as a first step for accurate one-step PET quantification, Nucl. Med. Commun. 35 (3) (2014) 316–324.

[23] C.J. Punt, M. Buyse, C.H. Kohne, P. Hohenberger, R. Labianca, H.J. Schmoll, et al., Endpoints in adjuvant treatment trials: a systematic review of the literature in colon cancer and proposed definitions for future trials, J. Natl. Cancer Inst. 99 (13) (2007) 998–1003.

[24] M. Rota, L. Antolini, M.G. Valsecchi, Optimal cut-point definition in biomarkers: the case of censored failure time outcome, BMC Med. Res. Methodol. 15 (2015) 24.

[25] J. Zugazagoitia, A.B. Enguita, J.A. Nunez, L. Iglesias, S. Ponce, The new IASLC/ATS/ERS lung adenocarcinoma classification from a clinical perspective: current concepts and future prospects, J. Thorac. Dis. 6 (Suppl. 5) (2014) S526–36.

[26] W.D. Travis, E. Brambilla, A.P. Burke, A. Marx, A.G. Nicholson, F.T. Bosman, E.S. Jaffe, S.R. Lakhani, H. Ohgaki (Eds.), WHO Classification of Tumours of the Lung, Pleura, Thymus and Heart, 4th ed., IARC Press, Lyon, 2015.

[27] J. Cuaron, M. Dunphy, A. Rimner, Role of FDG-PET scans in staging, response assessment, and follow-up care for non-small cell lung cancer, Front. Oncol. 2 (2012) 208.

[28] C. Nahmias, W.T. Hanna, L.M. Wahl, M.J. Long, K.F. Hubner, D.W. Townsend, Time course of early response to chemotherapy in non-small cell lung cancer patients with 18F-FDG PET/CT, J. Nucl. Med. 48 (5) (2007) 744–751.

[29] C. Pottgen, S. Levegrun, D. Theegarten, S. Marnitz, S. Grehl, R. Pink, et al., Value of 18F-fluoro-2-deoxy-D-glucose-positron emission tomography/computed tomography in non-small-cell lung cancer for prediction of pathologic response and times to relapse after neoadjuvant chemoradiotherapy, Clin. Cancer Res. 12 (1) (2006) 97–106.

[30] J.S. Ryu, N.C. Choi, A.J. Fischman, T.J. Lynch, D.J. Mathisen, FDG-PET in staging and restaging non-small cell lung cancer after neoadjuvant chemoradiotherapy: correlation with histopathology, Lung cancer 35 (2) (2002) 179–187.

[31] R.J. Cerfolio, B. Ojha, S. Mukherjee, A.H. Pask, C.S. Bass, C.R. Katholi, Positron emission tomography scanning with 2-fluoro-2-deoxy-d-glucose as a predictor of response of neoadjuvant treatment for non-small cell carcinoma, J. Thorac. Cardiovasc. Surg. 125 (4) (2003) 938–944.

[32] R.J. Cerfolio, A.S. Bryant, T.S. Winokur, B. Ohja, A.A. Bartolucci, Repeat FDG-PET after neoadjuvant therapy is a predictor of pathologic response in patients with non-small cell lung cancer, Ann. Thorac. Surg. 78 (6) (2004) 1903-9; discussion 9.

[33] M. Schmucking, R.P. Baum, R. Bonnet, K. Junker, K.M. Muller, Correlation of histologic results with PET findings for tumor regression and survival in locally advanced non-small cell lung cancer after neoadjuvant treatment, Der Pathologe 26 (3) (2005) 178–189.

[34] F. Lococo, C. Galeone, D. Formisano, S. Bellafiore, A. Filice, T. Annunziata, et al., 18F-fluorodeoxyglucose positron emission tomographic scan in solid-type p-stage-I pulmonary adenocarcinomas: what can produce false-negative results? Eur. J. Cardiothorac. Surg. 51 (4) (2017) 667–673.

[35] H. Vesselle, A. Salskov, E. Turcotte, L. Wiens, R. Schmidt, C.D. Jordan, et al., Relationship between non-small cell lung cancer FDG uptake at PET, tumor histology, and Ki-67 proliferation index, J. Thorac. Oncol. 3 (9) (2008) 971–978.

[36] H.J. Jeong, J.J. Min, J.M. Park, J.K. Chung, B.T. Kim, H.J.M. Jeong, et al., Determination of the prognostic value of [(18)F]fluorodeoxyglucose uptake by using positron emission tomography in patients with non-small cell lung cancer, Nucl. Med. Commun. 23 (9) (2002) 865–870.

[37] R.J. Downey, T. Akhurst, M. Gonen, A. Vincent, M.S. Bains, S. Larson, et al., Preoperative F-18 fluorodeoxyglucose-positron emission tomography maximal standardized uptake value predicts survival after lung cancer resection, J. Clin. Oncol. 22 (16) (2004) 3255–3260.

[38] R.J. Cerfolio, A.S. Bryant, B. Ohja, A.A. Bartolucci, The maximum standardized uptake values on positron emission tomography of a non-small cell lung cancer predict stage, recurrence, and survival, J. Thorac. Cardiovasc. Surg. 130 (1) (2005) 151–159.

[39] S.M. Eschmann, G. Friedel, F. Paulsen, M. Reimold, T. Hehr, W. Budach, et al., Is standardised (18)F-FDG uptake value an outcome predictor in patients with stage III non-small cell lung cancer? Eur. J. Nucl. Med. Mol. Imaging 33 (3) (2006) 263–269.

[40] S. Mukhopadhyay, M.D. Feldman, E. Abels, R. Ashfaq, S. Beltaifa, N.G. Cacciabeve, et al., Whole slide imaging versus microscopy for primary diagnosis in surgical pathology: a multicenter blinded randomized noninferiority study of 1992 cases (Pivotal study), Am. J. Surg. Pathol. 42 (1) (2018) 39–52.

[41] G. Litjens, C.I. Sanchez, N. Timofeeva, M. Hermsen, I. Nagtegaal, I. Kovacs, et al., Deep learning as a tool for increased accuracy and efficiency of histopathological diagnosis, Sci. Rep. 6 (2016) 26286.

[42] B. Ehteshami Bejnordi, M. Veta, P. Johannes van Diest, B. van Ginneken, N. Karssemeijer, G. Litjens, et al., Diagnostic assessment of deep learning algorithms for detection of lymph node metastases in women with breast cancer, JAMA 318 (22) (2017) 2199–2210.

[43] G. Campanella, M.G. Hanna, L. Geneslaw, A. Miraflor, V. Werneck Krauss Silva, K.J. Busam, et al., Clinical-grade computational pathology using weakly supervised deep learning on whole slide images, Nat. Med. 25 (8) (2019) 1301–1309.

[44] N. Coudray, P.S. Ocampo, T. Sakellaropoulos, N. Narula, M. Snuderl, D. Fenyo, et al., Classification and mutation prediction from non-small cell lung cancer histopathology images using deep learning, Nat. Med. 24 (10) (2018) 1559–1567.

[45] K.H. Yu, C. Zhang, G.J. Berry, R.B. Altman, C. Re, D.L. Rubin, et al., Predicting non-small cell lung cancer prognosis by fully automated microscopic pathology image features, Nat. Commun. 7 (2016) 12474.

[46] O. Sertel, J. Kong, H. Shimada, U.V. Catalyurek, J.H. Saltz, M.N. Gurcan, Computer-aided prognosis of neuroblastoma on whole-slide images: classification of stromal development, Pattern Recognit. 42 (6) (2009) 1093–1103.

[47] D. Bychkov, N. Linder, R. Turkki, S. Nordling, P.E. Kovanen, C. Verrill, et al., Deep learning based tissue analysis predicts outcome in colorectal cancer, Sci. Rep. 8 (1) (2018) 3395.

[48] A.H. Beck, A.R. Sangoi, S. Leung, R.J. Marinelli, T.O. Nielsen, M.J. van de Vijver, et al., Systematic analysis of breast cancer morphology uncovers stromal features associated with survival, Sci. Transl. Med. 3 (108) (2011) 108ra13.